Sensors and Actuators A 263 (2017) 113–121

Contents lists available at ScienceDirect

Sensors and Actuators A: Physical

journal homepage: www.elsevier.com/locate/sna

Low-frequency active noise control of an underwater large-scale structure with distributed giant magnetostrictive actuators

Wenjie Wang[a,b,*], P.J. Thomas[b]

[a] Fluid and Acoustic Engineering Laboratory, Beihang University, Beijing, People's Republic of China
[b] School of Engineering, University of Warwick, Coventry, CV4 7AL, United Kingdom

ARTICLE INFO

Article history:
Received 2 January 2017
Received in revised form 29 May 2017
Accepted 30 May 2017
Available online 3 June 2017

Keywords:
Underwater large-scale acoustic structure
Low frequency
Active noise control
Noise reduction
Giant magnetostrictive actuator

ABSTRACT

A light and thin underwater large-plate active acoustic structure is developed that satisfies the particular requirements of high pressure resilience, low frequency and high efficiency encountered in underwater work environments. A low-frequency miniaturized active control unit, with a thickness of less than 50 mm, is designed using giant magnetostrictive material (GMM). The noise reduction performance is measured with an active control system based on a multi-channel adaptive filter. The active control system is developed within a LabVIEW environment and can achieve significant levels of noise reduction within time intervals of less than one second achieving absorption coefficients far exceeding 0.8 even under high pressures. The new active-control system incorporates hardware and software components and represents a novel technology for low-frequency underwater noise reduction.

1. Introduction

Since the emergence of silent submarines, navies in the developed countries have primarily focused on noise detection frequencies substantially below 2 kHz. In recent years active detection sonars with substantially low frequencies have been used regularly. Low-frequency detection sound waves can not only achieve over the horizon (OTH) detection, but also lead to shell resonance, increase the target intensity, and overcome acoustic stealth. Thus, low frequency detection can leave the target fully exposed to the enemy in the monitoring system. It is of crucial importance for large scale targets to resolve this safety hazard at low frequency.

Traditional passive acoustic structures are unable of response to incoming low-frequency sound waves. This is due to sound reflection being governed by the material properties and the overall structure of the target. Active noise control techniques, however, offer an effective means to achieve low frequency noise reduction. Nevertheless, compared with the significant progress in the aerodynamic field, active noise control is hardly used in underwater acoustics due to its harsh application requirements such as high pressure, light weight and high efficiency. Low-frequency active control of a large-scale underwater target is rarely reported because of its special military background.

Structures for active noise control employing piezoelectric ceramics [1] and accelerometers for underwater targets are referred to as "Smart Tiles", this terminology was introduced by the Naval Civil Engineering Laboratory in 1996 [2–4]. Multifunctional active noise reduction structures can have many concurrent functions such as active sound absorption, active sound insulation and active sound radiation control [5]. Related research based on PVDF thin films and Sonopanel composite structures, resulted in the development of active acoustic structures for underwater targets. Two layers of PVDF thin films are used as signal separator to separate the incident wave and the reflected wave by means of a delay algorithm. The most efficient active noise- reduction effect can be achieved with these signals by active methods as described by Howarth et al. [6–8].

The most important component of signal separation and secondary sound source in active noise control are low-frequency acoustic transducers. Giant Magnetostrictive Materials (GMM) can be designed for piston-type underwater acoustic transducers. This low frequency active sonar can transmit signals of 200 Hz whose sound intensity is 200 dB [9,10]. Macro Fiber Composites are another new smart material for shell active noise control [11,12].

Frequently used materials are piezoelectric materials [13–16] (such as piezoelectric ceramics PZT, piezoelectric film PVDF) and magnetostrictive materials (such as rare earth material, giant magnetostrictive material). Nevertheless, the most common materials are piezoelectric ceramics. However, the disadvantages of ceramics are the required high driving voltage, small actuating amplitude, and the fragility of the material which limits its scope for underwa-

* Corresponding author at: Fluid and Acoustic Engineering Laboratory, Beihang University, Beijing, People's Republic of China.
E-mail address: wangwenjie@buaa.edu.cn (W. Wang).

http://dx.doi.org/10.1016/j.sna.2017.05.044
0924-4247/

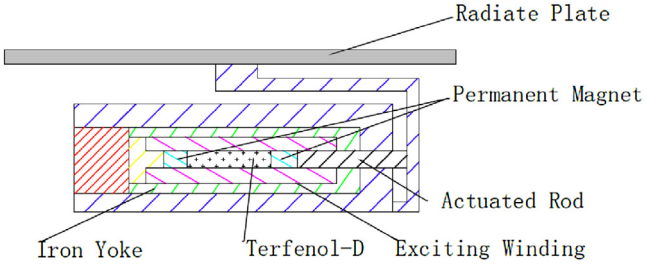

Fig. 1. GMA structure.

ter applications. Meanwhile, giant magnetostrictive material used in land high-frequency or ultra-high frequency transducer fields and GMM has problems associated with heat transfer and cooling [17–20]. Although GMM do not need to cooling in water, it is difficult to use them at low frequencies especially when the structural size of the Giant Magnetostrictive Actuator (GMA) is less than 50 mm.

In this paper, an active-control technology of an underwater large-scale target based on giant magnetostrictive materials is studied in the low-frequency range. A GMA was designed step by step to meet these requirements. The multi-channel control software was developed within a LabVIEW environment and achieves transient acoustic noise reduction. A limited area composed of active control units was used as the secondary sound source in a high pressure anechoic tank. The performance characteristics of the active noise control were evaluated by means of monitoring the reflection coefficients.

2. Active unit design method

The active unit used a giant magnetostrictive actuator which is based on the magnetostrictive effect. The basic parameters proposed in accordance with task requirements must be determined prior to the design of the magnetostrictive actuator. This section describes the design of an actuator which can improve on the weakness of piezoelectric ceramics such as fragility, low efficiency and high drive voltage.

2.1. Structure parameters of the active unit

Based on the design principle of an alternating current electromagnetic circuit, the giant magnetostrictive actuator under 2 kHz is designed with a Terfenol-D rod, as illustrated in Fig. 1, which can be applied to special requirements such as low frequency, high power and miniaturization.

Depending on the working conditions such as high pressure and current density, the diameter of the bare wire can be chosen from standard sizes. The diameter of the bare wire can be obtained from the current density. The magnetic circuit will be working repeatedly within short time intervals.

The coil thickness is:

$$e = \frac{H}{4\pi n_1 n_2 I} \tag{1}$$

where, H is the magnetic field intensity. n_1 and n_2 are the number of turns per unit length and the unit thickness of layers respectively. I is the current.

The outer radius of the coil is:

$$r_2 = r_1 + e + e_j(N_2 - 1) \tag{2}$$

where, r_1 and r_2 are the outer radius of the Terfenol-D rod and the outer radius of the coil respectively. e_j is the thickness of each layer of the insulation materials (e_j = 0.05 mm) and N_2 is the number of coil layers ($N_2 = e{\cdot}n_2$).

The total number of turns is:

$$N = (n_1 L_c)(n_2 e) \tag{3}$$

where, L_c is the length of the coil.

Set one end of the coil as the coordinate origin, the axis of the distribution of the magnetic field (approximation for multilayer coil) is:

$$H_x = 2\pi n_1 n_2 I\{(x+l)\ln\frac{r_2 + \left[r_2^2 + (x+l)^2\right]^{1/2}}{r_1 + \left[r_1^2 + (x+l)^2\right]^{1/2}} + (l-x)\ln\frac{r_2 + \left[r_2^2 + (x+l)^2\right]^{1/2}}{r_1 + \left[r_1^2 + (x+l)^2\right]^{1/2}} \tag{4}$$

where, H_x is the magnetic field at position x.

Due to the alternating current (AC) in the coil, the total impedance coil consists of two parts, that is the resistance and the inductance.

$$R = \rho_T \pi (r_1 + r_2) N / S_d \tag{5}$$

$$S_d = \frac{\pi}{4} d_n^2 \tag{6}$$

where, R is resistance. S_d is the effective cross-sectional area of the wire and d_n is the diameter of the bare wire. The resistance coefficient of the conductor is ρ_T = 0.01191.

The calculation to determine the self-induction coefficient is, in general, complex. However, for the particular case of a simple straight solenoid coil, as considered in this paper, the Biot-Savart law can be used to obtain an approximation of its value. Nevertheless, this approximation is larger than the actual value. This is so because the magnetic field of the coil is assumed to be uniform whereas the actual magnetic field is non-uniform and the discrepancy is particularly pronounced for short coils. Due to the existing edge effects the field strength near the ends of the coil is only half its center value.

The self-induction coefficient is:

$$L = \mu_0 N^2 V_c / L_c \tag{7}$$

where, μ_0 is the permeability of air, N is the total number of turns on the coil. V_c is the volume of the coil.

When the frequency of the alternating current within the coil is f, the impedance is

$$X_L = 2\pi f L \tag{8}$$

The total impedance of the coil is

$$Z = \sqrt{R^2 + X_L^2} \tag{9}$$

The required voltage and consumption power of the coil is:

$$U_m = IZ; \quad P_m = I^2 R \tag{10}$$

The bias magnetic field of permanent magnets is used to eliminate Second Harmonic Generation (SHG) of a Terfenol-D rod and provide mechanical movement of the Terfenol-D rod in a linear range. The calculations associated with the bias magnetic field are also very complex and the results obtained are generally not very accurate. For engineering application it is therefore a common procedure to use an estimate in the first instance and, thereafter, the actual measurement provides a reference for improvements. The estimate is obtained from the λ-H curve. If this estimate does not satisfy the requirements then the shape of the permanent magnet should be improved until the performance is satisfactory.

The design requirements and the steps outlined above define the geometric dimensions of the actuator. The diameter of radiation plate located in the end of the actuator drive rod is 150 mm and its

Table. 1
Parameters of Terfenol-D.

Magnetostrictive Coefficient ($\times 10^{-9}$ m/A)	2.0–3.2
Energy Density (/kJ m^{-3})	12–25
Resistivity ($\times 10^{-5}$ Ω cm)	6.0
Elasticity Modulus ($\times 10^{10}$ Pa)	2.5–3.5
Density (/g cm^{-3})	9.25
Relative Permeability	3–15

thickness is 2 mm. The total thickness of the GMA is only 40 mm which is ideal for thin low-frequency acoustic smart materials.

2.2. Finite element simulation

Finite element analysis uses a mathematical approximation method to simulate the real physical condition such as geometry and loading conditions. We have conducted a finite element analysis, employing the ANSYS 14.0 software, to simulate our experiments computationally. and provide theoretical support for the structural design and optimization. The GMA parameters are shown in Table 1.

In Fig. 2, the element type used the three dimensional solid element *solid 186* in finite element model of ANSYS 14.0. The axial key parts including rare earth rods, driver, permanent magnets and other components used more than 200,000 elements to guarantee the accuracy in the modeling process of meshing, which can influence the GMA modal frequencies.

The boundary conditions of the finite element model are that the shell is constrained in all degrees of freedom and the axial parts have axial freedom. The mode extraction method of Block Lanczos in ANSYS 14.0 is adopted to calculate the first four orders of resonance frequencies between 100 Hz–3 kHz. The results of the simulations are compared to the experimental data in Fig. 3.

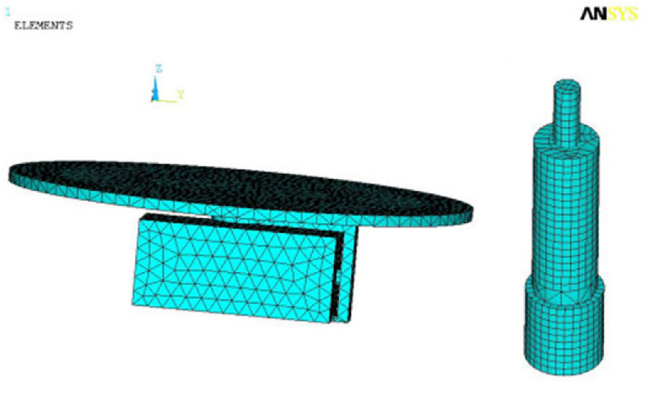

Fig. 2. GMA mesh.

Table 2
Results of simulation and experiment (Hz).

	1st frequency	2nd frequency	3rd frequency	4th frequency
Simulation	303.77	765.91	1270.9	2815.0
Experiment	296.30	879.41	1562.5	2963.8

For comparison, the resonance frequencies of the GMA is measured by a laser scanning vibrometer (type: MLV-100). The experimental and computational results display, overall, identical trends, as shown in Table 2. This indicates that the experimental values are overall consistent with the theoretical ones.

2.3. Absorption coefficients testing

The sound absorption of the GMA unit is measured in the water-filled acoustic tube, illustrated in Fig. 4, by means of a set of adaptive

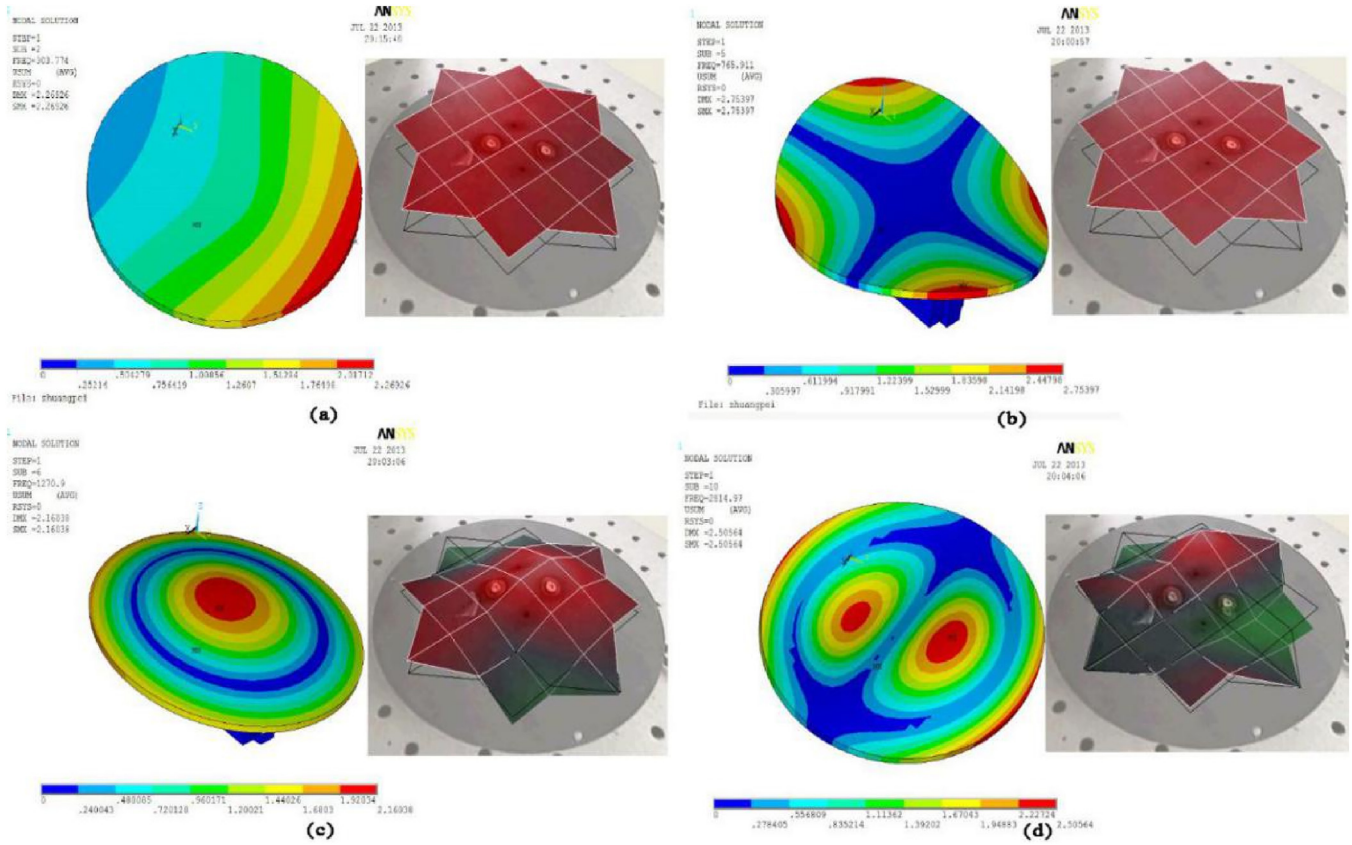

Fig. 3. Results of simulation and experiment.

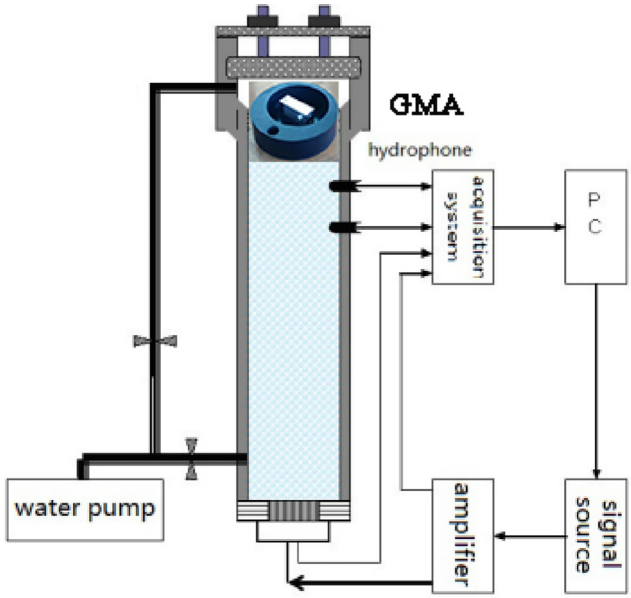

Fig. 4. GMA unit and acoustic tube.

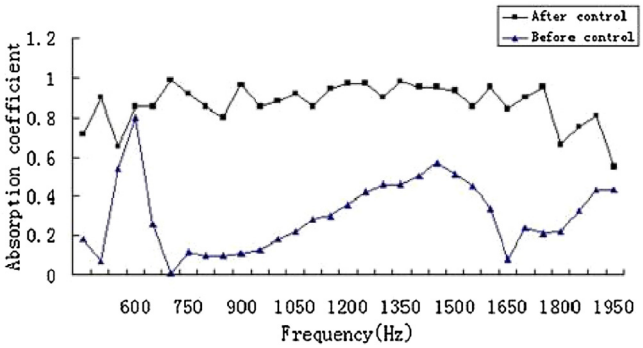

Fig. 5. Absorption coefficients of GMA unit.

control systems. The frequencies of the incident acoustic signal ranged from 500 Hz to 2 kHz at the bottom of the acoustic tube. Sensors at the top of the tube receive the reflected sound waves from the surface of the GMA unit. Therefore, the sound absorption performance of the GMA unit can be evaluated, and the acoustic field can be displayed by means of an oscilloscope. The reflection coefficient of the water-air interface is close to 1.0. The sound absorption coefficients of the GMA unit before and after control are shown in Fig. 5.

Fig. 5 reveals that, compared with sound absorption coefficients of the GMA unit before control, the coefficients after control are much higher. The average value of the coefficient after control lies above 0.85. The GMA units have a broadband noise reduction effect. In the low frequency range the sound absorption performance of the GMA far exceeds the traditional passive absorption structures.

3. Active large plate design method and active control system

3.1. Active large plate

A large-plate sound source was used as a secondary source, or anti-source, which is constructed by uniformly distributed GMA units as shown in Fig. 6. These GMA units are embedded in rubber material. This plate specimen size is 1 m × 1 m × 50 mm with 8 mm steel backing.

Fig. 6. Active large plate.

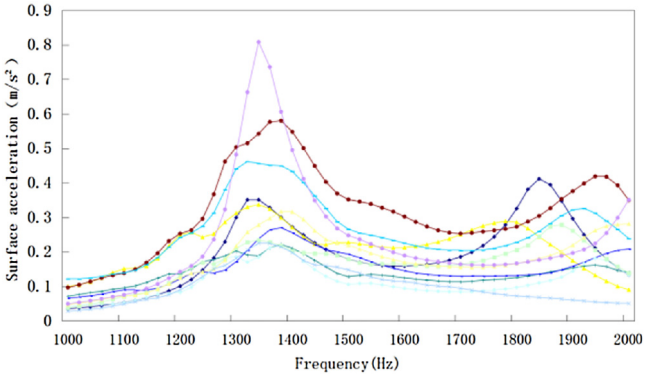

Fig. 7. Surface accelerations of GMA units.

The surface acceleration of these sixteen units were measured by means of a surface vibration analyzer (type: B&K 2513) and they were adjusted to the same phase. In Fig. 7 all units display the same trends of the frequency response characteristics. The main resonance frequency band ranges from 1.1 kHz to 2 kHz which is in accordance with the initial design purpose and application frequency band.

3.2. Active control system

An active control theory has been developed adequately in the field of aerodynamics. The D-LMS algorithm in Eq. (11) is widely used in many active control methods [21]. The active control system is developed based on the LabVIEW and DLMS layout illustrated in Fig. 8.

$$W(n+1) = W(n) - 2\mu e(n)X(n-k_s) \tag{11}$$

The primary microphone or hydrophone measures the signal $x(n)$ from the primary source and the error sensor monitors the error signal $e(n)$. When the error signal is reduced to the minimum through an adaptive filter algorithm, noise reduction is achieved. The active control system has three branches (Background And Parameter Set, Impulse response of the secondary-path and ANC System) as shown in Fig. 10.

4. Experiment apparatus and testing procedure

The active noise control experiments were conducted in an anechoic tank with a diameter of 4.5 m and a length of 25 m. The

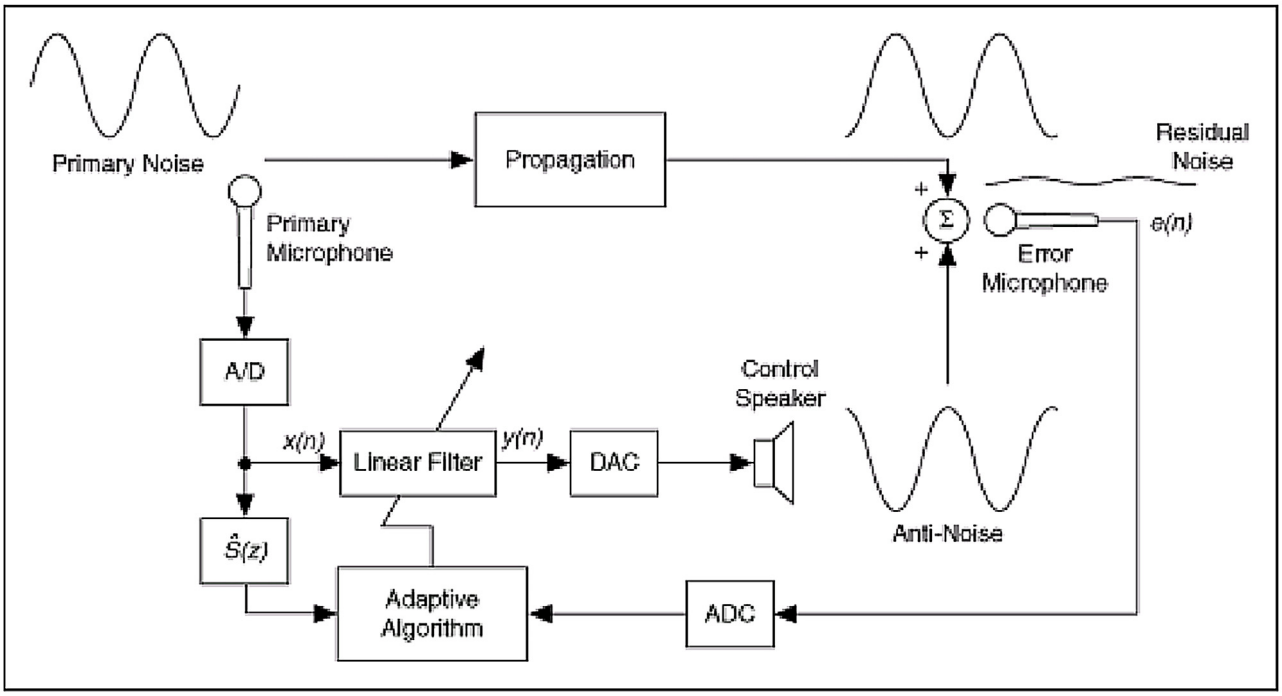

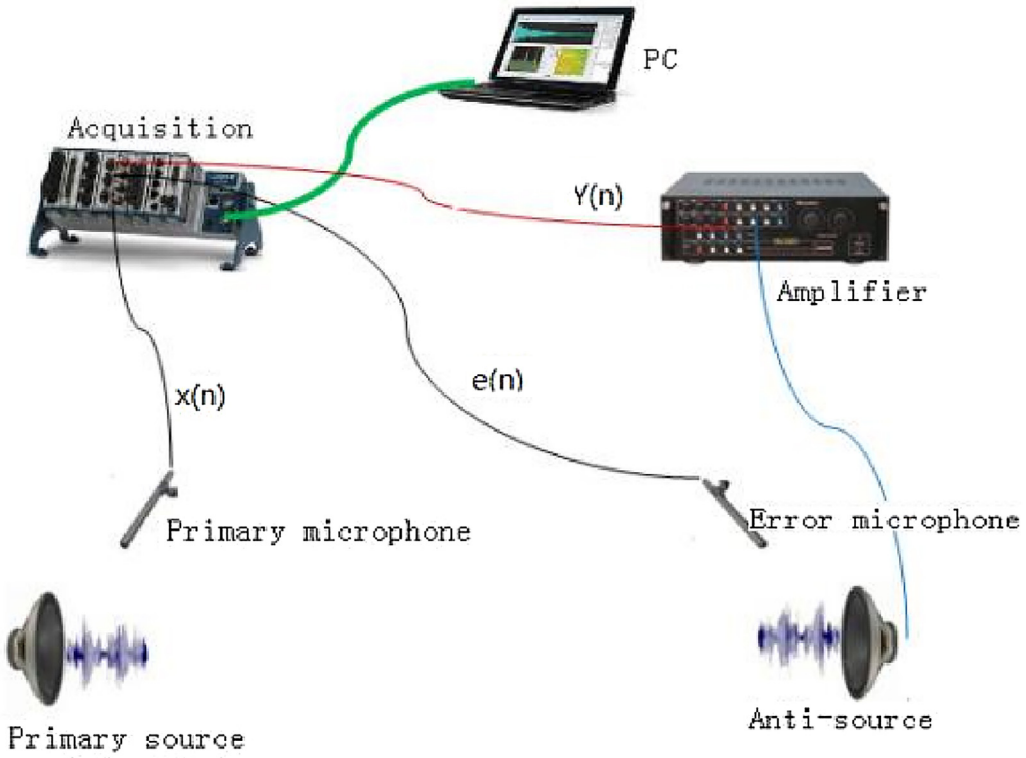

Fig. 8. Active control procedure.

primary source used 127 circular array sound sources. The plate sound source is the secondary source or anti-source. The whole performance testing system is shown in Fig. 9. After the signals were emitted from the primary source, the signal can be separated to get the incident signal and the reflected signal in the plate sound source. The controller analyzed and calculated the incident signal to send a secondary signal to the GMA units with the multi-channel DLMS algorithm.

In order to evaluate active echo suppression performance under the condition of low frequencies, sound wave from primary sound noise source ranged from 500 Hz to 3 kHz. The entire testing process was conducted under atmospheric pressure and for a hydrostatic pressure of 1 MPa. High hydrostatic pressure was achieved by water

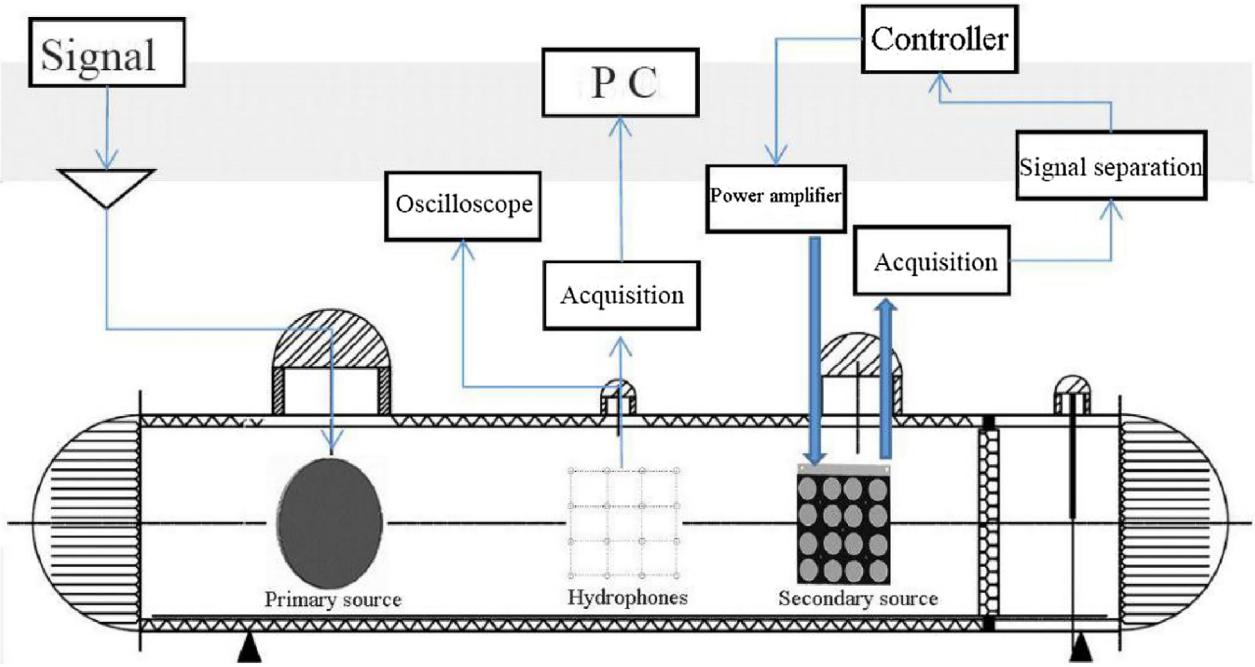

Fig. 9. Experiment system.

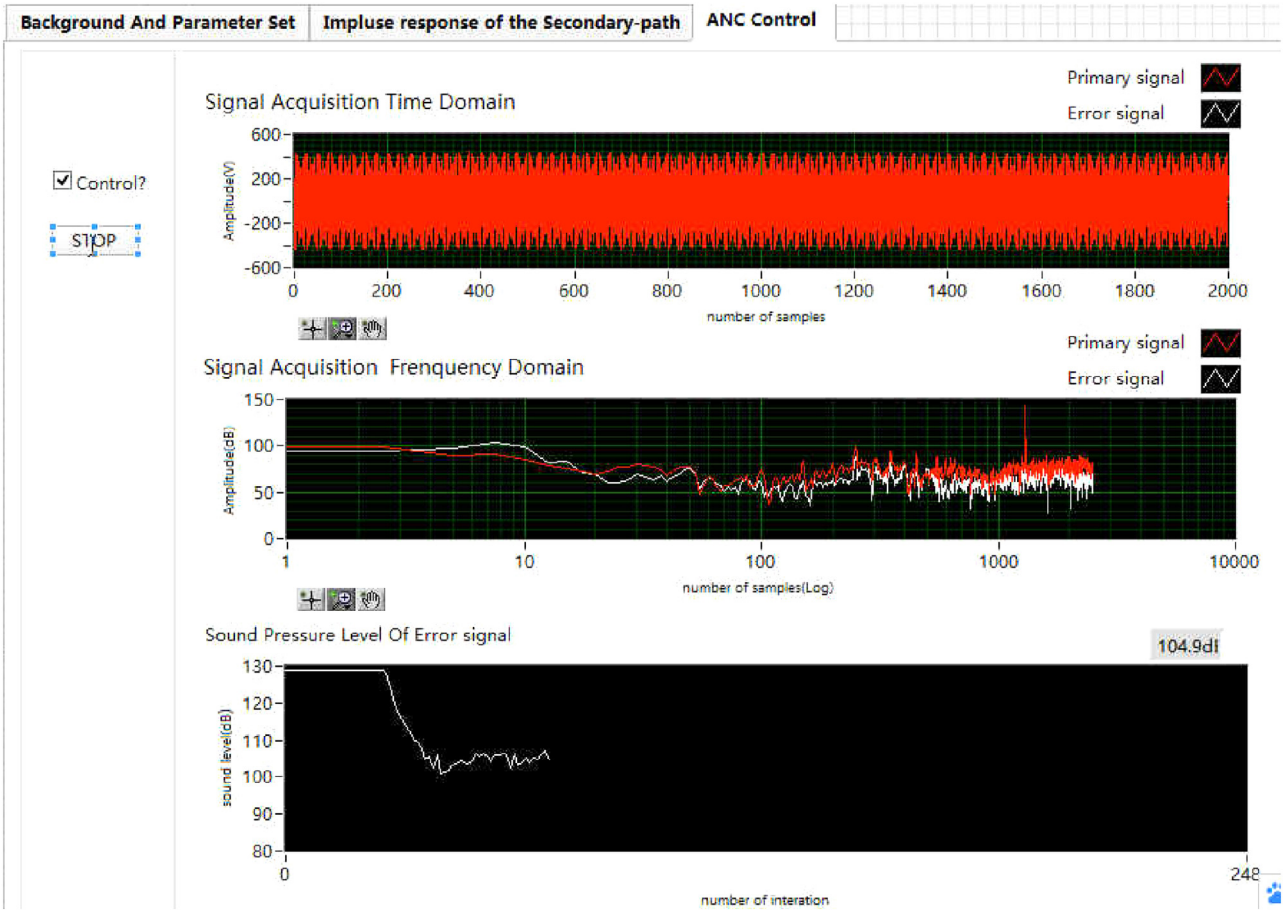

Fig. 10. Testing process (f = 1.3 kHz). A) Absorption coefficients of 0 MPa. B) Absorption coefficients of 0.96 MPa.

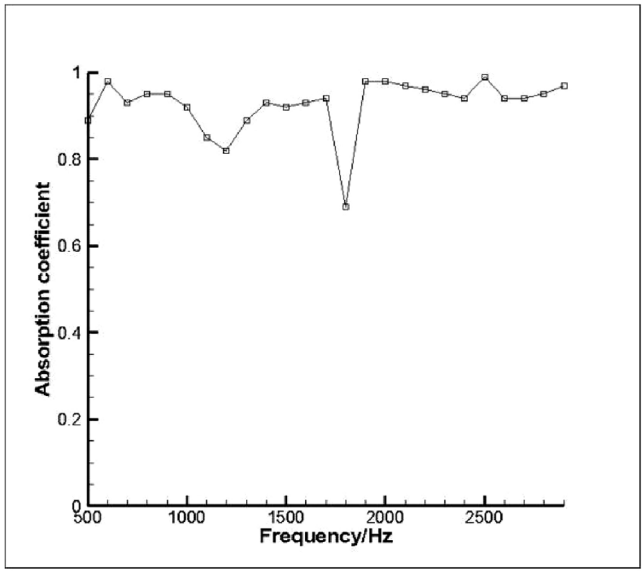

A) Absorption coefficients of 0 MPa.

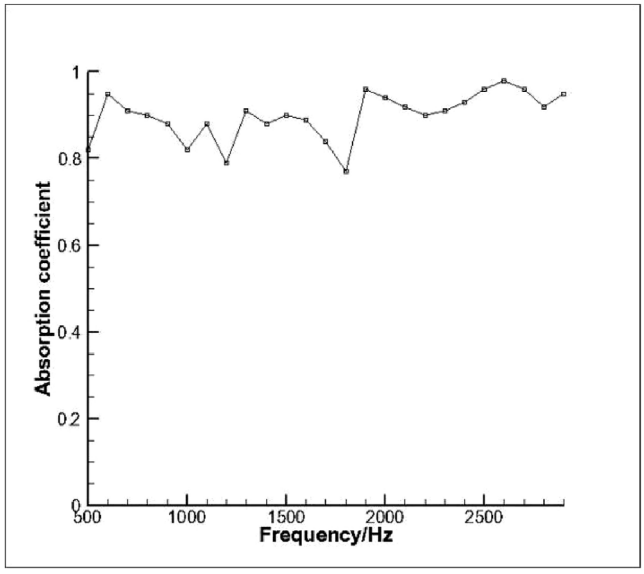

B) Absorption coefficients of 0.96 MPa.

Fig. 11. Absorption coefficients of large plate.

injection. After the secondary acoustic signals interfered with primary signals, the hydrophones can monitor the acoustic stealth effect. In each monitor position, the oscilloscope will display local signals in real time.

Prior to the experiments the tank was sealed and water was injected to increase the hydrostatic pressure to 1 MPa. The active noise control experiments were carried out at the stable pressure value of 0.96 MPa. The active control process is shown in Fig. 10. There are three spectra in Fig. 10. The first spectrum displays the time-domain results, the second spectrum shows the frequency-domain results and the third spectrum is the sound absorption coefficient of the active noise control. In the first and second spectrum, the red line is the primary signal from a signal generator (type: Agilent 33220A) and the white line is the secondary sound signal. The sound pressure level of the error signal reduced from 128 dB to 103 dB when the incident frequency was 1.3 kHz. The convergence time of the total active control was less than 1 s. The time domain and frequency domain of the signal can be found in Fig. 10 and the current frequency is clearly displayed in the frequency domain.

In the frequency band from 500 Hz to 3 kHz, under atmospheric pressure, the active absorption coefficients of the large target in the large pressure anechoic tank is substantially higher than 0.9 at constant temperature as shown in Fig. 11. Meanwhile, the absorption coefficients under high pressure is slightly smaller than those under hydrostatic pressure in Fig. 5. But these values are still more than 0.8 and the average coefficient was about 0.9.

Along with the absorption coefficient, the acoustical transmission property is also validated through the hydrophone array in Fig. 9. The sound pressure levels in front and back of the active plate sample are shown in Fig. 12. The distance from the hydrophone array to the active plate is 50 cm. The hydrophone array is com-

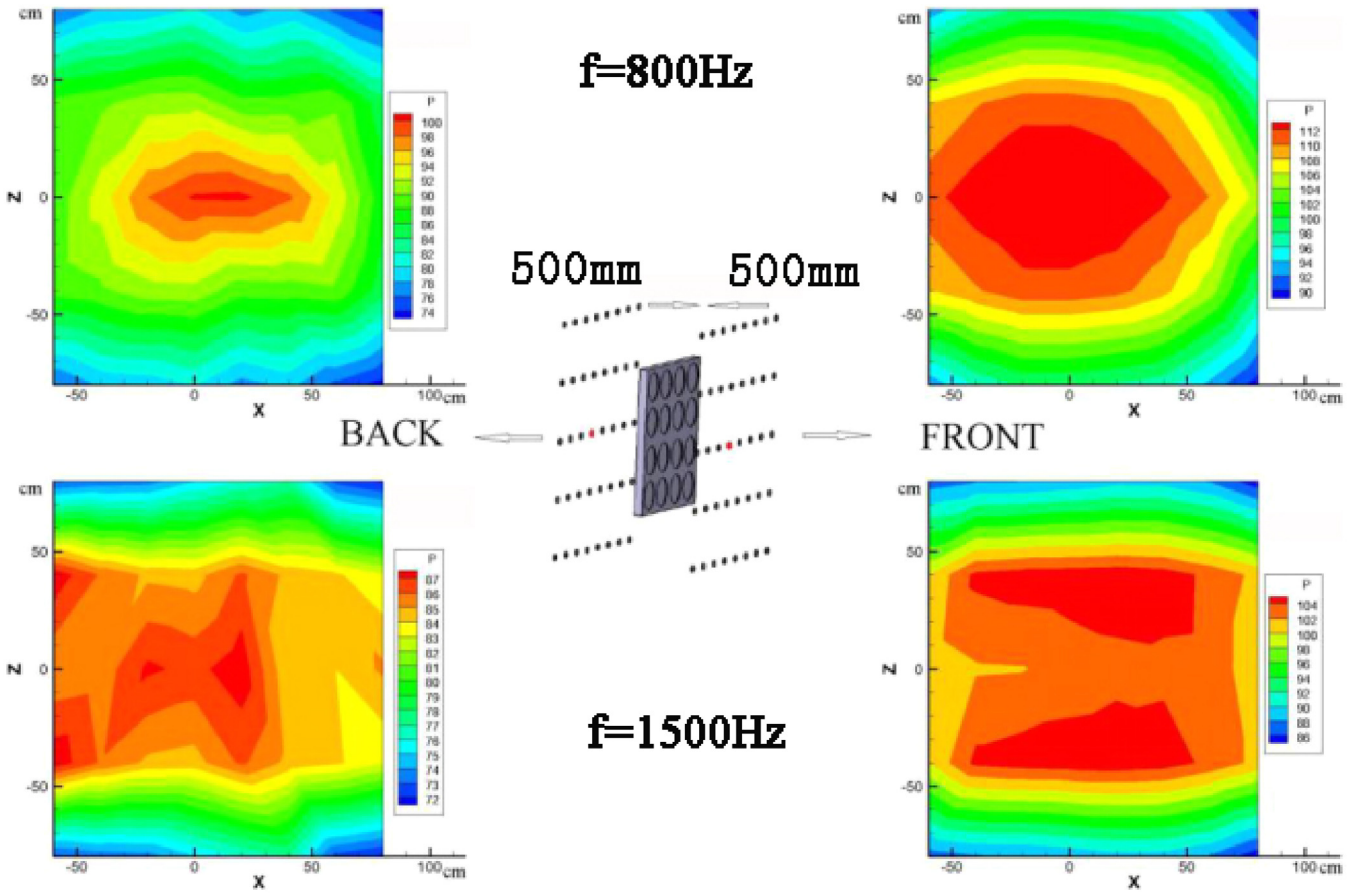

Fig. 12. Array signals of front and back.

posed of 16 hydrophones. The horizontal distance between two hydrophones is 20 cm and the longitudinal distance between two hydrophones is 0.40 m. The hydrophone marked in red at Location [3,4] in the array is at the center point of the plate.

The acoustic fields of 800 Hz and 1500 Hz are shown in Fig. 12. The bright area is off-center due to the relative position. Because the array is close to the active plate, acoustic signals from the array are near field signals of the plate. The controlled area is an approximate rectangle which is the region of active units. The sound pressure level of the transmission attenuation is more than 10 dB even 20 dB through 58 mm at low frequencies. It has a substantial control effect even if the frequency is as low as 800 Hz.

5. Conclusion and discussion

In this paper, a thin low-frequency actuator with GMM was designed to satisfy special underwater requirements. A large active acoustic structure was constructed with distributed giant magnetostrictive actuators. An integrated underwater active control system based on LabVIEW was proposed to achieve low frequency noise reduction even in deep water or under high pressure. This large acoustic structure with high absorption coefficients can provide a very important reference in the context of the design of underwater equipment.

The objective of the present work was to evaluate the potential engineering application of the acoustic characteristics of a large-scale underwater acoustic structure with giant magnetostrictive actuators in the low frequency band. This large acoustic structure consisted of GMA units that can provide useful results in active noise reduction. To distinguish this from traditional passive noise reduction methods the current research with high absorption coefficients has a certain reference value for the underwater acoustical noise reduction. Meanwhile, experiments under high pressure indicate this work has the potential to be used for underwater operation even in deep water. All these underwater active control experiments are the very important works which indicate that the exploratory in the lab can be used in the engineering application.

Future research will evaluate the active noise reduction performance under higher pressure ($\lesssim$5 MPa) and at other temperatures. Additionally, a monitoring system will be built to observe the noise reduction effect of the whole space. Experiments in lakes and in shallow seas would be beneficial in order to achieve more realistic conditions mirroring real engineering applications.

Acknowledgment

This paper is supported by the China Postdoctoral Science Foundation (No. 2016M591046).

References

[1] J.F. Tressler, R.E. Newnham, W.J. Hughes, Capped ceramic underwater sound projector: the cymbal transducer, J. Acoust. Soc. Am. 105 (1999) 591–600.
[2] R.D. Corsaro, B. Houston, J. Bucaro, Sensor actuator tile for underwater surface impedance control studies, J. Acoust. Soc. Am. 102 (1997) 1573–1581.
[3] R.D. Corsaro, B.H. Houston, Sensor actuator panels for underwater acoustic control, Proc. SPIE 2779 (1996) 598–602.
[4] R.D. Corsaro, B.H. Houston, J.D. Klunder, Integrated smart actuator containing a monolithic conformed accelerometer, Proc. SPIE 3044 (1997) 397–405.
[5] F.D. Shields, L.D. Lafleur, Smart acoustically active surfaces, J. Acoust. Soc. Am. 102 (1997) 1559–1566.
[6] T.R. Howarth, V.K. Varadan, X.Q. Bao, V.V. Varadan, Piezocomposite coating for active underwater sound reduction, J. Acoust. Soc. Am. 2 (1991) 823–831.

[7] T.R. Howarth, X.Q. Bao, V.V. Varadan, Digital time delay network for an active underwater acoustic coating, J. Acoust. Soc. Am. 3 (1993) 1613–1619.
[8] T.R. Howarth, Y.T. Robert, Electroacoustic evaluations of 1–3 piezocomposite SonoPanel materials, IEEE Trans. Ultrason. Ferroelectr. Freq. Control 47 (2000) 886–894.
[9] G. Engdahl, Handbook of Giant Magnetostrictive Materials, Academic Press, San Diego, 2000.
[10] J.H. Goldie, M.J. Gerver, J. Oleksy, Composite terfenol-D sonar transducers, Proc. SPIE 3675 (1999) 223–234.
[11] W.K. Wilkie, R.G. Bryant, J.W. High, et al., Low-cost piezocomposite actuator for structural control applications, Proc. SPIE 3991 (2000) 323–334.
[12] R.B. Williams, D.J. Inman, M.R. Schultz, et al., Nonlinear tensile and shear behavior of macro fiber composite actuators, J. Compos. Mater. 38 (2004) 855–869.
[13] Z.W. Chen, J.Q. Hu, Piezoelectric and dielectric properties of Bi0.5(Na0.84K0.16)0.5 TiO3-Ba(Zr0.01Ti0.96)O3 lead free piezoelectric ceramics, Adv. Appl. Ceram. 107 (2008) 222–226.
[14] Huang Shouqing, Yang Yong, Liu Shouwen, Chu Xiangcheng, A large-diaphragm piezoelectric panel loudspeaker and its acoustic frequency response simulation method, Appl. Acoust. 125 (2017) 176–183.
[15] Montazer Babak, Sarma Utpal, Modeling and analysis the effect of PZT area on square shaped substrate for power enhancement in MEMS piezoelectric energy harvester, J. Circuits Sys. Comput. 26 (2017) 9–21.
[16] Yuan Xi, Zhu Song, Li Xianfang, Mechanical performance of piezoelectric fiber composites and electroelastic field concentration near the electrode edges, Mater. Des. 128 (2017) 71–79.
[17] Zhu Yuchuan, Ji Liang, Theoretical and experimental investigations of the temperature and thermal deformation of a giant magnetostrictive actuator, Sen. Actuators A: Phys. 218 (2014) 167–178.
[18] Zhou Can, Duan Jian, Deng Guiling, Li Junhui, Improved thermal characteristics of a novel magnetostrictive jet dispenser using water-cooling approach, Appl. Therm. Eng. 112 (2017) 1–7.
[19] L.F. Cótica, S. Betal, C.T. Morrow, Thermal effects in magnetoelectric properties of NiFe2O4/Pb(Zr0.52Ti0.48)O3/NiFe2O4tri-layered composite, Integr. Ferroelectr. 174 (2016) 203–209.
[20] Sun Jianping, Wang Jianxin, Structure design and verification of thermo-acoustic refrigerator driven by magnetostrictive transducer, Mod. Electron. Tech. 39 (2016) 164–167.
[21] H.S. Kim, Y. Park, Delayed-XLMS algorithm: an efficient ANC algorithms utilizing robustness of cancellation path mode, J. Sound Vib. 212 (1998) 875–887.

Biographies

Dr. Wenjie Wang was born in Shandong, China, in 1988. He received the Ph.D. degree in fluid and acoustic engineering from Beihang University, Beijing, China, in 2015. He is now a postdoc in Fluid and Acoustic Engineering Laboratory, Beihang University. His main research interests include underwater acoustics, aeroacoustics, intelligent systems with smart materials and structures, piezoelectric devices and nonlinear dynamics.

Dr. Peter J. Thomas was born in Rotenburg a. d. Fulda, Germany, in 1960. He received the Dipl.-Phys. and Dr. rer. nat. degrees from the Georg-August-Universität in Göttingen, Germany, in 1988 and 1991, respectively. He is currently a Professor at the School of Engineering, University of Warwick, Coventry, UK where he is also the Director of their Fluid Dynamics Research Centre. His research interests include Rotating Flows, Laminar-Turbulent Transition, Vortex Stability, Oceanographic Coastal Currents, Granular Flows and Particle-Laden Flows. Over the years, he has received more than $4 M in research funds from funding agencies and industry, and published more than 150 journal and conference papers.